Journal of Hazardous Materials 184 (2010) 704–709

Contents lists available at ScienceDirect

Journal of Hazardous Materials

journal homepage: www.elsevier.com/locate/jhazmat

Synthesis, characterization and adsorptive performance of $MgFe_2O_4$ nanospheres for SO_2 removal

Ling Zhao [a], Xinyong Li [a,c,*], Qidong Zhao [a], Zhenping Qu [a], Deling Yuan [a], Shaomin Liu [b], Xijun Hu [c], Guohua Chen [c]

[a] Key Laboratory of Industrial Ecology and Environmental Engineering and State Key Laboratory of Fine Chemical, School of Environmental Sciences and Technology, Dalian University of Technology, Dalian 116024, China
[b] Department of Chemical Engineering, Curtin University of Technology, Perth, WA 6845, Australia
[c] Department of Chemical and Biomolecular Engineering, The Hong Kong University of Science & Technology, Clear Water Bay, Kowloon, Hong Kong, China

ARTICLE INFO

Article history:
Received 30 March 2010
Received in revised form 25 August 2010
Accepted 25 August 2010
Available online 22 September 2010

Keywords:
SO_2 removal
$MgFe_2O_4$
Nanospheres

ABSTRACT

A type of uniform Mg ferrite nanospheres with excellent SO_2 adsorption capacity could be selectively synthesized via a facile solvothermal method. The size of the $MgFe_2O_4$ nanospheres was controlled to be 300–400 nm in diameter. The structural, textural, and surface properties of the adsorbent have been fully characterized by a variety of techniques (Brunauer–Emmett–Teller, BET; X-ray diffraction analysis, XRD; scanning electron microscopy, SEM; and energy-dispersive X-ray spectroscopy, EDS). The valence states and the surface chemical compositions of $MgFe_2O_4$ nanospheres were further identified by X-ray photoelectron spectroscopy (XPS). The behaviors of SO_2 oxidative adsorption on $MgFe_2O_4$ nanospheres were studied using Fourier transform infrared spectroscopy (FTIR). Both the sulfite and sulfate species could be formed on the surface of $MgFe_2O_4$. The adsorption equilibrium isotherm of SO_2 was analyzed using a volumetric method at 298 K and 473 K. The results indicate that $MgFe_2O_4$ nanospheres possess a good potential as the solid-state SO_2 adsorbent for applications in hot fuel gas desulfurization.

1. Introduction

Sulfur dioxide is one of the major pollutants released to the atmosphere as a result of volcanic activity and the combustion of fuels in power plants, factories, houses and transportation. It is a corrosive gas which can be harmful to the environment and human health. Today, many international agencies regulate air quality in the environment. Therefore, a variety of methods have been proposed and developed for the removal of sulfur compounds. Recently, the most popular and inexpensive method receiving much attention for SO_x removal is the addition of selective sorbents [1,2], notably metal oxides.

A considerable amount of research has been conducted on the suitability of various metal oxides for SO_2 removal. CaO-based sorbents have been the leading candidate materials for several decades. However, they are not suitable enough because the materials require a very high temperature for the removal of SO_2 and their reuse is nearly impossible due to the very stable $CaSO_4$ formed during SO_2 adsorption. Al_2O_3-based sorbents showed low SO_x removal capacity because the $Al_2(SO_4)_3$ formed is very unstable at the regenerator temperature. It releases the sulfate species as produced in the SO_x adsorption condition [3]. MgO-based sorbents have been reported as a high potential sorbents for SO_2 removal, especially in the presence of oxidation promoters. Many promoters were added to the MgO in order to promote the SO_2 transformation to SO_3, which would be easily absorbed into the MgO [3–5]. Different material promoters have been claimed as SO_2 oxidation promoters [3–6], and cerium oxide has been proved as an excellent candidate [7–10]. However, cerium oxide is not used widely mainly for its high cost. For this reason, instead of cerium the use of iron was proposed. The iron has the ability to play a dual role, as an oxidizing and a reducing catalyst.

Recently, Mg–Fe-based sorbents enjoy a special attention for their effective adsorption of SO_2. Lee et al. [11] have demonstrated that Ce–Fe–Mg-based sorbents showed excellent sulfur removal capacity and regeneration ability. Wang et al. [12] have investigated an Mg–Fe–Al–O mixed oxide with spinel structure. Podworny et al. [13] have explained the behaviors of MgO–$MgFe_2O_4$ spinels in gaseous environment having high concentration of sulfur oxides. However, the conventional preparation techniques can easily lead to the production of agglomerated particles with irregular shape, which limit their absorption capacity for SO_2. Therefore, it is very important and desirable to control the synthesis procedures to

* Corresponding author at: Key Laboratory of Industrial Ecology and Environmental Engineering and State Key Laboratory of Fine Chemical, School of Environmental Sciences and Technology, Dalian University of Technology, Dalian 116024, China. Tel.: +86 411 8470 7733; fax: +86 411 8470 8084.
E-mail address: xyli@dlut.edu.cn (X. Li).

0304-3894/$ – see front matter © 2010 Elsevier B.V. All rights reserved.
doi:10.1016/j.jhazmat.2010.08.096

achieve particles with uniform size distribution and well dispersion.

In this paper, a type of uniform Mg ferrite nanospheres with tunable diameter in the range of 300–400 nm were prepared via a facile solvothermal method, and evaluated as potential SO_2 sorbent using a volumetric method. To obtain more information about $MgFe_2O_4$ nanospheres surface after its interaction with sulfur dioxide, a comparative XPS and FTIR spectra study was conducted.

2. Experimental

2.1. Preparation of materials

All the chemicals in this work, such as hydrated iron chloride ($FeCl_3{\cdot}6H_2O$), magnesium chloride ($MgCl_2{\cdot}6H_2O$), ammonium acetate ($NH_4{\cdot}Ac$), and ethylene glycol, were analytical grade regents from the Beijing Chemical Reagents Factory and used as starting materials without further purification.

The typical preparation procedure of $MgFe_2O_4$ nanospheres is as follows [14]. $FeCl_3{\cdot}6H_2O$ (6 mmol) and $MgCl_2{\cdot}6H_2O$ (3 mmol) were added into ethylene glycol (90 ml) to form a clear solution. Then a protective agent $NH_4{\cdot}Ac$ (45 mmol) was added into the solution to form a mixture under vigorous stirring at room temperature. Subsequently, the mixture was put into a Teflon lined stainless steel autoclave of 120 ml capacity and sealed and maintained at 180 °C for 24 h. Finally, the system was allowed to cool to room temperature naturally. The obtained black precipitate was collected by filtration, washed with absolute ethanol and distilled water in sequence for several times, and dried in a vacuum drying box at 80 °C overnight. The final product was calcined at 600 °C for 4 h. The sample was labeled as $MgFe_2O_4$ nanospheres.

As a comparison, another type of $MgFe_2O_4$ was prepared by the coprecipitation method as follows [15]. An aqueous solution (100 ml) containing $MgCl_2{\cdot}6H_2O$ (0.05 mol) and $FeCl_3{\cdot}6H_2O$ (0.1 mol). The mixed metal salt solution and the NaOH (6 mol/l) solution were simultaneously added to a glass reactor and mixed under vigorous mechanical stirring, with the pH maintained between 9 and 10. Then, the mixture was heated at 90 °C for 18 h. The precipitate was washed several times with absolute ethanol and deionized water and dried at 80 °C overnight. The final product was calcined at 600 °C for 4 h, and labeled as $MgFe_2O_4$-CP.

2.2. Characterization of materials

The obtained samples were characterized on a Rigaku D/Max 2550VB/PC X-ray powder diffractometer (XRD) with a Cu Kα radiation source (k = 0.154056 nm), and operated at a voltage of 40 kV and a current of 100 mA.

Scanning electron microscopy (SEM) was performed on a JEOLJSM-6360LV microscope. Chemical composition of the particles was determined by energy-dispersive spectrometry (EDS).

N_2 physisorption was performed on a Quantachrome Autosorb 1 instrument to study specific surface area, pore volume, and pore size distribution. Samples were pretreated by degassing at 120 °C overnight to remove any adsorbed species.

XPS data were recorded using a Perkin-Elmer PHI 5600 electron spectrometer using acrochromatic Al Kα radiation (1486.6 eV) with Ar^+ sputtering to remove the surface layer of the sample. The binding energies and intensities were calculated after subtraction of a Shirley-type background from raw photoemission spectra. Complex spectra in the Fe2p region were resolved into four components: two for the Fe (III) and two for the Fe (II) oxidation states (see below), according to a fitting procedure described elsewhere [16].

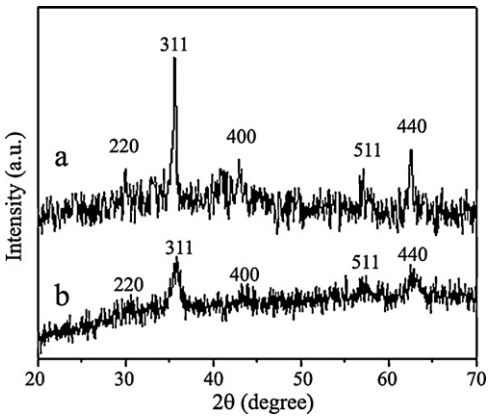

Fig. 1. XRD patterns of fresh $MgFe_2O_4$-CP and $MgFe_2O_4$ nanospheres: (a) $MgFe_2O_4$-CP sample and (b) $MgFe_2O_4$ nanspheres sample.

FTIR spectra were recorded on a VERTEX 70-FTIR equipped with a smart collector and a MCT/A detector cooled by liquid N_2.

2.3. Activity test

The adsorption equilibrium isotherm of SO_2 was analyzed using a volumetric method at 298 K and 473 K [17]. The method was based on the mole balance of SO_2 gas in a closed system. UHP grade SO_2 gas was used for the measurement. For each test, the amount of the $MgFe_2O_4$ adsorbent was 0.1 g.

3. Results and discussion

3.1. Characterization of samples

The wide angle XRD patterns of the fresh $MgFe_2O_4$ nanospheres and the $MgFe_2O_4$-CP are shown in Fig. 1. The XRD patterns obtained from the two samples exhibit similar characteristics, which are in good agreement with the standard diffraction patterns of $MgFe_2O_4$ (JCPDS 73-2410). The diffraction peaks corresponding to planes (2 2 0), (3 1 1), (4 0 0), (5 1 1) and (4 4 0) provide a clear evidence for the formation of spinel structure of the $MgFe_2O_4$. Compared with the $MgFe_2O_4$-CP, the diffraction peaks of $MgFe_2O_4$ nanospheres are wider and its intensity becomes lower. The mean crystallite sizes of the $MgFe_2O_4$ nanospheres and the $MgFe_2O_4$-CP are 6.1 and 20.8 nm respectively, calculated from the broadening of the (3 1 1) XRD peaks of $MgFe_2O_4$ phase according to the Scherrer formula: $D = 0.89\lambda/\beta\cos\theta$ [18].

SEM analysis of the $MgFe_2O_4$-CP (see Fig. 2(a)) reveals that the sample consists of microparticles with irregular morphology, and the particle size varies in a wide range. By contrast, the $MgFe_2O_4$ nanospheres are in spherical shape with smooth surfaces and are uniform in size with diameters ranging from 300 nm to 400 nm (Fig. 2(b)). The origin of the morphological difference between the two types of samples most likely lies in their respective preparation method. The EDX spectra results from the two samples indicate that samples only contain Mg, Fe, O (Fig. 2(c) and (d)).

Fig. 3 shows the N_2 adsorption/desorption isotherms of the $MgFe_2O_4$ nanospheres and the $MgFe_2O_4$-CP. All the profiles reveal a small hysteresis loop, implying the presence of mesopores at high relative pressure range between 0.6 and 0.9 (Type IV) [19]. Moreover, the N_2 adsorption quantity for the $MgFe_2O_4$ nanospheres sample is much higher than that for the $MgFe_2O_4$-CP, indicating the abundance of mesopores in the $MgFe_2O_4$ nanospheres. The isotherm of $MgFe_2O_4$ nanospheres exhibits a high Type IV adsorption/desorption shape with an H1 hysteresis loop, which implies that the synthesized $MgFe_2O_4$ nanospheres consist of com-

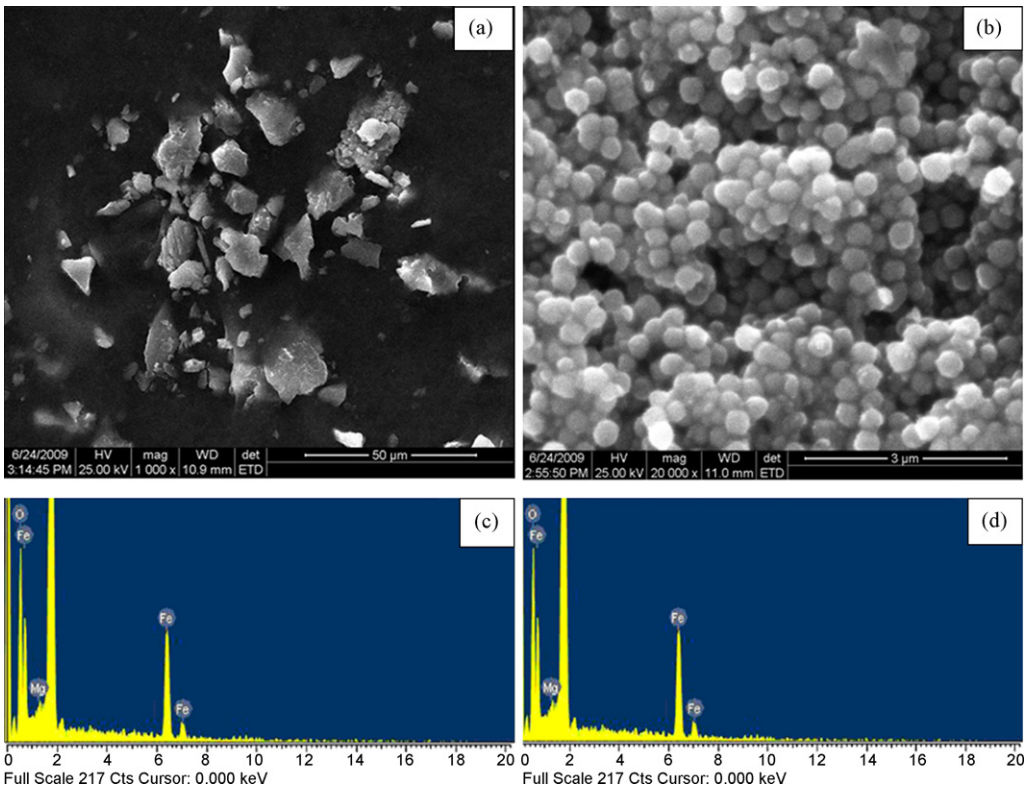

Fig. 2. SEM and EDS of fresh $MgFe_2O_4$-CP and $MgFe_2O_4$ nanospheres. (a) SEM of fresh $MgFe_2O_4$-CP; (b) SEM of fresh $MgFe_2O_4$ nanospheres; (c) EDS of fresh $MgFe_2O_4$-CP; (d) EDS of fresh $MgFe_2O_4$ nanospheres.

pacts of approximately uniform particles in a fairly regular way with a narrow range of pore size distribution [20,21]. However, for $MgFe_2O_4$-CP sample, a H3 hysteresis loop was observed, indicating that aggregates of plate-like structures exist [21]. Besides, the amount of adsorbed N_2 by the sample is neglectable, which shows its lower adsorption ability. We also find that the $MgFe_2O_4$ nanospheres possess high specific surface area and total pore volume (116 m^2/g and 0.32 cm^3/g), while the $MgFe_2O_4$-CP sample shows only 9.02 m^2/g of specific surface area and 0.017 cm^3/g of total pore volume (see Table 1). It is well known that the specific surface area could vary depending upon the crystallite size and shape. Therefore, the comparison of both parameters could explain the low specific surface area of $MgFe_2O_4$-CP in addition to its larger particle size, as observed in SEM analysis (see Fig. 2(a)).

The profiles of pore size distribution are given in the inset of Fig. 3. It could be observed that for the $MgFe_2O_4$ nanospheres, the pore size distribution is peaked around 10 nm with a substantial percentage of pores sized below 5.0 nm. Meanwhile, for the $MgFe_2O_4$-CP sample, an almost flattened profile of pore size distribution is observed, which indicates that nonporous structure is obtained by the coprecipitation method.

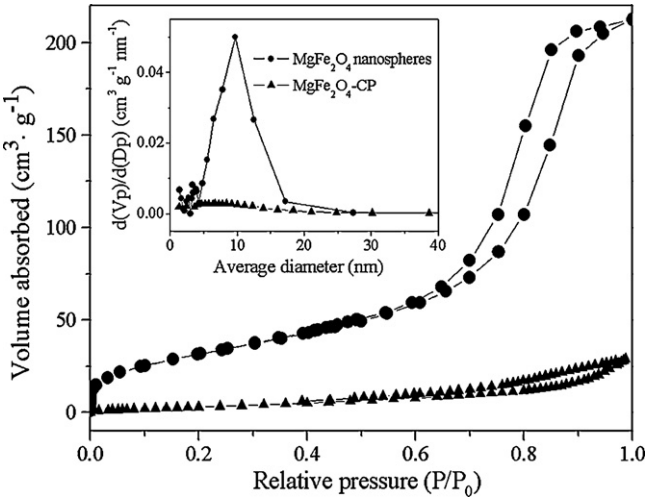

Fig. 3. N_2 adsorption/desorption isotherm and BJH pore size distribution of fresh $MgFe_2O_4$-CP and $MgFe_2O_4$ nanospheres.

3.2. Adsorption of SO_2

Fig. 4 shows the adsorption isotherms of SO_2 in the $MgFe_2O_4$ nanospheres and the $MgFe_2O_4$-CP sample at 298 K and 473 K. It is seen that the adsorption capacity of $MgFe_2O_4$ nanospheres is much higher than that of the $MgFe_2O_4$-CP sample. This suggests that the $MgFe_2O_4$ nanospheres should be a better adsorbent for SO_2 abatement. The adsorption capacity is consistent with the specific surface area of the adsorbent. The specific surface area of the $MgFe_2O_4$ nanospheres (116 m^2/g) is much higher than that of the $MgFe_2O_4$-CP sample (9.02 m^2/g). Moreover, a substantial percentage of pores for $MgFe_2O_4$ nanospheres is now in the quasi-micropore region (below 5 nm), and molecules may be adsorbed following the micropore-filling mechanism before they enter the pore body. Because the pore opening is smaller than the pore body,

Table 1
Structural parameters of the fresh $MgFe_2O_4$ nanospheres and $MgFe_2O_4$-CP.

Sample	S_{BET}[a] (m^2/g)	Total volume[b] (cm^3/g)
$MgFe_2O_4$ nanospheres	116	0.32
$MgFe_2O_4$-CP	9.02	0.017

[a] BET surface area calculated from the linear part of the BET plot.
[b] Single-point total pore volume of pores at $P/P_0 = 0.99$.

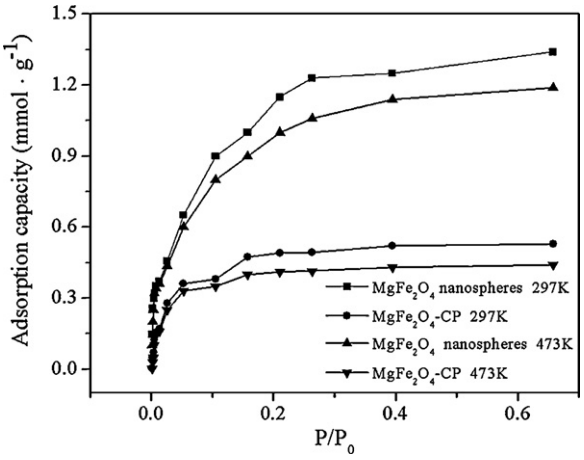

Fig. 4. Adsorption isotherm of SO_2 in various adsorbents at 298 K and 473 K.

molecules will have difficulty in escaping once they have been adsorbed into the pore body. Therefore, $MgFe_2O_4$ nanospheres have much higher SO_2 adsorption capacity than the $MgFe_2O_4$-CP sample.

3.3. XPS studies

Metal oxide based adsorbents are usually consisted of at least two active metal oxides as it is found that mixed metal oxides generally display better redox properties than single one [22–24]. To obtain more surface chemical information about the $MgFe_2O_4$ nanospheres after their interaction with sulfur dioxide, a comparative XPS and FTIR spectra investigation was carried out subsequently. Fig. 5 presents S2p spectra taken from $MgFe_2O_4$ nanospheres after its interaction with sulfur dioxide at 473 K. One can see that the treatment of the $MgFe_2O_4$ nanospheres by SO_2 results in an appearance of S2p features. To analyze these spectra in more detail and to apply literature data for comparison, we deconvoluted the S2p lines into two components. The comparison with literature data allows unambiguous assignment of these $S2p_{3/2}$ features to sulfite (167.5–168.5) and sulfate (168.9–169.1) species [25–27]. As seen from Fig. 5, the banding energy of $S2p_{3/2}$ on $MgFe_2O_4$ nanospheres locates at 168.3 eV and 169.5 eV, which are in good agreement with SO_3^{2-} and SO_4^{2-} states, respectively. Therefore, the $MgFe_2O_4$ nanosphere surface contains a certain amount of both sulfite and sulfate species after the adsorption of SO_2.

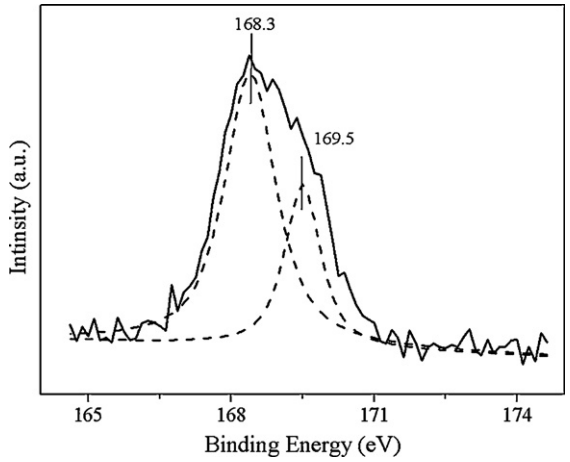

Fig. 5. The S2p photoemission spectra recorded after the treatment of $MgFe_2O_4$ nanospheres with SO_2 at 473 K.

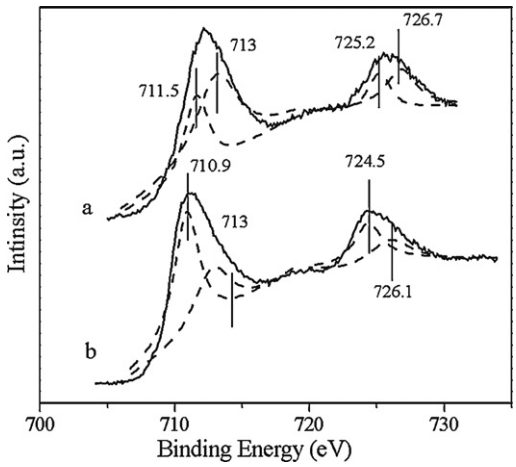

Fig. 6. The Fe2p photoemission spectra recorded for (a) fresh $MgFe_2O_4$ nanospheres and (b) $MgFe_2O_4$ nanospheres adsorbed with SO_2 at 473 K.

The sulfation of $MgFe_2O_4$ nanospheres is also exhibited in the behavior of the Mg1s and Fe2p (or Fe3p) lines. The parameters of the Mg1s line change negligibly under the reaction (not shown here), indicating the permanency in the chemical state of magnesium ions. Contrary to magnesium, a part of the Fe (III) ions transform into the Fe (II) ions as a result of the interaction of the $MgFe_2O_4$ surface with pure SO_2.

As mentioned in Section 2, the Fe2p spectra have a complex structure composed of one $Fe2p_{3/2}/Fe2p_{1/2}$ doublet from Fe (III) ions and one doublet from Fe (II) ones. Fig. 6 shows the Fe2p spectra together with their deconvolution belonging to the Fe (III) and Fe (II) states. The $Fe2p_{3/2}$ lines, characteristic of the Fe (III) oxidation state, are located at 713 eV (both initial $MgFe_2O_4$ nanospheres surface and used $MgFe_2O_4$ nanospheres surface). The $Fe2p_{1/2}$ lines, characteristic of the Fe (III) oxidation state, are located at 726.7 eV (initial $MgFe_2O_4$ nanospheres surface) and 726.1 eV (used $MgFe_2O_4$ nanospheres surface). Moreover, the $Fe2p_{3/2}$ lines, characteristic of the Fe (II) oxidation state, are located at 711.5 eV (initial $MgFe_2O_4$) and 710.9 eV (used $MgFe_2O_4$). The $Fe2p_{1/2}$ lines, characteristic of the Fe (II) oxidation state, are located at 725.2 eV (initial $MgFe_2O_4$) and 725.5 eV (used $MgFe_2O_4$). Analysis of the Fe2p spectra indicates that the amount of Fe (III) ions is decreased as well as the Fe (II) ions being increased after the reaction with SO_2, which indicates that parts of Fe (III) ions in the catalysts are reduced to Fe (II) ions.

The interchanging between different oxidation states of transition metals could play an important role in SO_2 removal. It has been well known that CeO_2 can donate its lattice oxygen to SO_2 [28]. Smirnov et al. [29] have demonstrated that the sulfation of the CeO_2 is accompanied by a reduction of Ce (IV) ions to Ce (III) ones. Thus it is reasonable to deduce that the oxidation state of Fe can interchange between 3^+ and 2^+ to receive or donate oxygen for SO_2 molecules to adsorb on. Moreover, it has been known from Fig. 5 that both sulfite and sulfate species are formed on the surface after $MgFe_2O_4$ is exposed with SO_2. Therefore, it should allow us to conclude that the sulfation and reduction of iron proceed in parallel.

3.4. FTIR studies

The FTIR spectra of fresh $MgFe_2O_4$ nanospheres sample and sulfated sample in the range 4000–800 cm^{-1} are shown in Fig. 7. The spectrum clearly shows a broad absorption around 3430 cm^{-1}, which is a characteristic stretching vibration of hydroxylate (O–H). Peaks localized at 1623 cm^{-1} and 1411 cm^{-1} are assigned to

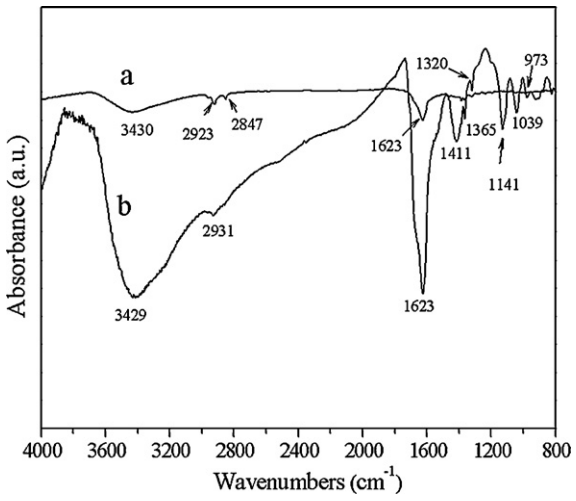

Fig. 7. IR spectra of adsorbed SO_2 on (a) fresh $MgFe_2O_4$ nanospheres and (b) $MgFe_2O_4$ nanospheres adsorbed with SO_2 at 473 K.

asymmetrical and symmetrical stretching vibration of carboxylate (O–C–O), respectively.

The 1411 cm^{-1} (broad), 1365 cm^{-1} (shoulder) and 1320 cm^{-1} (shoulder) characterize the formation of surface sulfate species with S=O bond. It has been shown already that the introduction of larger amounts of sulfates on $A1_2O_3$, TiO_2 or ZrO_2 shifts the highest frequency band near 1380 cm^{-1} to higher wavenumbers [30,31]. Wu et al. [32] also have found that a noticeable fact was a distinct shift of the sulfate band from 1346 cm^{-1} to 1364 cm^{-1}, which may be caused by the accumulation of sulfate species by the reaction of $SO_2 + O_2$ with Ag/Al_2O_3. Luo et al. [33] compared the peak of adsorbed SO_2 at 1345 cm^{-1} with gaseous SO_2 (at 1151 cm^{-1} and 1362 cm^{-1}) and SO_3 (at 1061 cm^{-1} and 1391 cm^{-1}). Moreover, when a very large amount of surface sulfate species is formed, another component appears near 1400 cm^{-1}, attributed to chemisorbed SO_3 like species [30,34]. The main band at 1141 cm^{-1} with shoulders at 1039 and 973 may be attributed to the symmetric stretching sulfite vibrations [35,36]. These results imply that sulfite and sulfate species can be formed on the surface of $MgFe_2O_4$, which is in good agreement with our XPS results.

4. Conclusion

A type of uniform Mg ferrite nanospheres with excellent SO_2 adsorption capacity could be selectively synthesized via a facile solvothermal method. Compared with the $MgFe_2O_4$ prepared by the coprecipitation method, $MgFe_2O_4$ nanospheres are controllable to be 300–400 nm in diameter and have much higher surface area and pore volume. These results suggest that the $MgFe_2O_4$ nanospheres should be a better adsorbent for SO_2 abatement. Both results from XPS and FTIR reveal that sulfite and sulfate species can be formed on the surface of $MgFe_2O_4$, and sulfites can be oxidized to sulfates at the expense of Mg ferrite, while Fe (III) is partially reduced to Fe (II). It is revealed that the sulfation and reduction of iron proceed in parallel during the SO_2 abatement.

Acknowledgements

This work was supported financially by the National Nature Science Foundation of China (nos. 20837001 and 20877013), the National High Technology Research and Development Program of China (863 Program) (nos. 2007AA061402 and 2009AA062604) and the Major State Basic Research Development Program of China (973 Program) (no. 2007CB613306).

References

[1] H. Dathe, A. Jentys, P. Haider, E. Schreier, R. Fricke, J.A. Lercher, On the trapping of SO_x on CaO–Al_2O_3-based novel high capacity sorbents, Phys. Chem. Chem. Phys. 8 (2006) 1601–1613.
[2] H.H. Tseng, M.Y. Wey, Y.S. Liang, K.H. Chen, Catalytic removal of SO_2, NO and HCl from incineration flue gas over activated carbon-supported metal oxides, Carbon 41 (2003) 1079–1085.
[3] Y. Wang, Z. Liu, L. Zhan, Z. Huang, Q. Liu, J. Ma, Performance of an activated carbon honeycomb supported V_2O_5 catalyst in simultaneous SO_2 and NO removal, Chem. Eng. Sci. 59 (2004) 5283–5290.
[4] T. Johannessen, S. Koutsopoulos, One-step flame synthesis of an active Pt/TiO_2 catalyst for SO_2 oxidations—a possible alternative to traditional methods for parallel screening, J. Catal. 205 (2001) 404–408.
[5] J. Dawody, M. Skoglundh, E. Fridell, The effect of metal oxide additives (WO_3, MoO_3, V_2O_5, Ga_2O_3) on the oxidation of NO and SO_2 over Pt/Al_2O_3 and $Pt/BaO/Al_2O_3$ catalysts, J. Mol. Catal. A 209 (2004) 215–225.
[6] J.A. Wang, A.L. Zhu, C.L. Li, Pathway of the cycle between the oxidative adsorption of SO_2 and the reductive decomposition of sulfate on the $MgAl_{2-x}Fe_xO_4$, J. Mol. Catal. A 139 (1999) 31–41.
[7] M.S.P. Carla, A.H. Cristiane, A.N. Arnaldo, L.F.M. Jose, Synthesis, characterization and evaluation of CeO_2/Mg Al-mixed oxides as catalysts for SO_x removal, J. Mol. Catal. A 241 (2005) 184–193.
[8] J.A. Wang, L.F. Chen, R. Limas-Ballesteros, Evaluation of crystalline structure and SO_2 storage capacity of a series of composition sensitive De-SO_2 catalysts, J. Mol. Catal. A 194 (2003) 181–193.
[9] X. Lin, W.F. Schneider, B.L. Trout, Chemistry of sulfur oxides on transition metals. III. Oxidation of SO_2 and self-diffusion of O, SO_2, and SO_3 on Pt (1 1 1), J. Phys. Chem. B 108 (2004) 13329–13340.
[10] M.Y. Smirnov, A.V. Kalinkin, A.V. Pashis, A.M. Sorokin, A.S. Noskov, K.C. Kharas, V.I. Bukhtiyarov, Interaction of Al_2O_3 and CeO_2 surfaces with SO_2 and $SO_2 + O_2$ studied by X-ray photoelectron spectroscopy, J. Phys. Chem. B 109 (2005) 11712–11715.
[11] S.J. Lee, S.Y. Jung, S.C. Lee, H.K. Jun, C.K. Ryu, J.C. Kim, SO_2 removal and regeneration of MgO-Based sorbents promoted with titanium oxide, Ind. Eng. Chem. Res. 48 (2009) 2691–2696.
[12] J. Wang, Z. Zhu, C. Li, Roles of cerium oxide and the reducibility and recoverability of the surface oxygen species in the $CeO_2/MgAl_2O_4$ catalysts, J. Mol. Catal. A: Chem. 139 (1999) 31–41.
[13] J. Podworny, J. Piotrowski, J. Wojsa, Investigations into the kinetics and mechanism of gas–solid state processes in MgO–MgR_2O_4 (R: Al, Cr, Fe) spinels–SO_2–O_2 system, Ceram. Int. 34 (2008) 1587–1593.
[14] A. Yan, X. Liu, R. Yi, R. Shi, N. Zhang, G. Qiu, Selective synthesis and properties of monodisperse Zn ferrite hollow nanospheres and nanosheets, J. Phys. Chem. C 112 (2008) 8558–8563.
[15] J. Amighian, M. Mozaffari, B. Nasr, Preparation of nano-sized manganese ferrite ($MnFe_2O_4$) via coprecipitation method, Phys. Stat. Sol. 9 (2006) 3188–3192.
[16] M. Romeo, K. Bak, J.E. Fallah, F.L. Normand, L. Hilaire, XPS study of the reduction of cerium dioxide, Surf. Interface Anal. 20 (1993) 508–512.
[17] X. Hu, B. King, D.D. Do, Ternary desorption and displacement kinetics of gases in activated carbon, Gas Sep. Purif. 8 (1994) 187–190.
[18] H.P. Klug, L.E. Alexander, in: H.P. Klug, L.E. Alexander (Eds.), Crystallite Size and Lattice Strains from Line Broadening, in X-ray Diffraction Procedures for Polycrystalline and Amorphous Materials, 2nd ed., John Wiley & Sons, New York, 1974, pp. 618–708.
[19] J.G. Yu, L.J. Zhang, B. Cheng, Y.R. Su, Hydrothermal preparation and photocatalytic activity of hierarchically sponge-like macro-/mesoporous titania, J. Phys. Chem. C 111 (2007) 10582–10589.
[20] M. Kruk, M. Jaroniec, Gas adsorption characterization of ordered organic–inorganic nanocomposite materials, Chem. Mater. 13 (2001) 3169–3183.
[21] K.S.W. Sing, D.H. Everett, R.A.W. Haul, L. Moscou, R.A. Pierotti, J. Rouquerol, T. Siemieniewska, Reporting physisorption data for gas/solid systems with special reference to the determination of surface area and porosity, Pure Appl. Chem. 57 (1985) 603–619.
[22] A.R. Grapain, J.A. Alatorre, A.G. Cortes, G. Diaz, Catalytic properties of a CuO–CeO_2 sorbent catalyst for de-SO_x reaction, Catal. Today 107–108 (2005) 168–174.
[23] M.F. Stephanopoulos, T. Zhu, Y. Li, Ceria based catalysts for the recovery of elemental sulfur from SO_2 laden gas streams, Catal. Today 62 (2000) 145–158.
[24] J.F. Akyurtlu, A. Akyurtlu, Behavior of ceria–copper oxide sorbent under sulfation conditions, Chem. Eng. Sci. 54 (1999) 2991–2997.
[25] N.R. Urban, K. Ernst, S. Bernasconi, Addition of sulfur to organic matter during early diagenesis of lake sediments, Geochim. Cosmochim. Acta 63 (1999) 837–853.
[26] J. Casanovas, J. Ricart, F. Millas, The interpretation of X-ray photoelectron spectra of pyrolized S-containing carbonaceous materials, Fuel 76 (1997) 1347–1352.
[27] D. Brion, Study by photoelectron spectroscopy of surface degradation of FeS_2, $CuFeS_2$, ZnS and PbS exposed to air and water, Appl. Surf. Sci. 5 (1980) 133–151.
[28] R.M. Ferrizz, R.J. Gorte, J.M. Vohs, TPD and XPS investigation of the interaction of SO_2 with model ceria catalysts, Catal. Lett. 82 (2002) 123–129.
[29] M.Y. Smirnov, A.V. Kalinkin, A.V. Pashis, A.M. Sorokin, A.S. Noskov, K.C. Kharas, V.I. Bukhtiyarov, Interaction of Al_2O_3 and CeO_2 surfaces with SO_2 and $SO_2 + O_2$ studied by X-ray photoelectron spectroscopy, J. Phys. Chem. B 109 (2005) 11712–11719.

[30] M. Waqif, O. Saur, J.C. Lavalley, S. Perathoner, G. Centi, Nature and mechanism of formation of sulfate species on copper/alumina sorbent-catalysts for sulfur dioxide removal, J. Phys. Chem. 95 (1991) 4051–4058.
[31] M. Waqif, J. Bachelier, O. Saur, J.C. Lavalley, Acidic properties and stability of sulfate-promoted metal oxides, J. Mol. Catal. 72 (1992) 127–138.
[32] Q. Wu, H.W. Gao, H. He, Conformational analysis of sulfate species on Ag/Al_2O_3 by means of theoretical and experimental vibration spectra, J. Phys. Chem. B 110 (2006) 8320–8324.
[33] T. Luo, J.M. Vohs, R.J. Gorte, An examination of sulfur poisoning on Pd/ceria catalysts, J. Catal. 210 (2002) 397–404.
[34] G. Centi, N. Passarini, S. Perathoner, Combined $DeSO_x/DeNO_x$ reactions on a copper on alumina sorbent-catalyst. 1. Mechanism of sulfur dioxide oxidation–adsorption, Ind. Eng. Chem. Res. 31 (1992) 1947–1955.
[35] Y. Ono, H. Tokunaga, T. Keii, Electron spin resonance study of sulfur dioxide $(1-)$ radicals on synthetic zeolites, J. Phys. Chem. 79 (1975) 752–756.
[36] Y. Ono, K. Suzuki, T. Keii, Electron spin resonance study of the formation of anion radicals over titanium exchanged Y-zeolite, J. Phys. Chem. 78 (1974) 218–220.